

WISE view of Narrow-Line Seyfert 1 galaxies: mid-infrared color and variability

Suwendu Rakshit^{1,2*}, Ansu Johnson^{2,3†}, C. S. Stalin², Poshak Gandhi⁴,
Sebastian Hoenig⁴

¹*Astronomy Program, Department of Physics and Astronomy, Seoul National University, Seoul 151-742, Republic of Korea*

²*Indian Institute of Astrophysics, Block II, Koramangala, Bangalore 560 034, India*

³*National Institute of Technology Tiruchirappalli - 620015*

⁴*Department of Physics & Astronomy, University of Southampton, Southampton, SO17 1BJ, UK*

ABSTRACT

We present the color and flux variability analysis at $3.4\ \mu\text{m}$ ($W1$ -band) and $4.6\ \mu\text{m}$ ($W2$ -band) of 492 narrow-line Seyfert 1 (NLSy1) galaxies using archival data from the Wide-field Infrared Survey Explorer (*WISE*). In the *WISE* color-color, ($W1 - W2$) versus ($W2 - W3$) diagram, $\sim 58\%$ of the NLSy1 galaxies of our sample lie in the region occupied by the blazar category of active galactic nuclei (AGN). The mean $W1 - W2$ color of candidate variable NLSy1 galaxies is 0.99 ± 0.18 mag. The average amplitude of variability is 0.11 ± 0.07 mag in long-term (multi-year) with no difference in variability between $W1$ and $W2$ -bands. The $W1 - W2$ color of NLSy1 galaxies is anti-correlated with the relative strength of [O III] to $H\beta$, strongly correlated with continuum luminosity, black hole mass, and Eddington ratio. The long-term amplitude of variability shows weak anti-correlation with the Fe II strength, continuum luminosity and Eddington ratio. A positive correlation between color as well as the amplitude of variability with the radio power at 1.4 GHz was found for the radio-detected NLSy1 galaxies. This suggests non-thermal synchrotron contribution to the mid-infrared color and flux variability in radio-detected NLSy1 galaxies.

Key words: galaxies: active - galaxies: Seyfert - techniques: photometric

1 INTRODUCTION

Active Galactic Nuclei (AGN) are the persistent luminous objects in the sky powered by accretion of matter onto the super-massive black holes (SMBHs) located at the centers of galaxies (Lynden-Bell 1969; Rees 1984). Models of AGN, in addition to the central SMBH, posit the presence of accretion disc surrounded by the dusty obscuring torus (Antonucci 1993; Urry & Padovani 1995), which are supported by the observed big blue bump (BBB) and mid-infrared (mid-IR) bump in their broad band spectral energy distribution (SED). The BBB is thought to be thermal emission from the accretion disk (Shakura & Sunyaev 1973) and the IR bump is from the dusty torus known from dust reverberation mapping studies (Suganuma et al. 2006; Koshida et al. 2014; Mandal et al. 2018). One of the important characteristics of AGN known since their discovery is that they

show flux variability (Ulrich et al. 1997; Wagner & Witzel 1995). This property of AGN, observed at different wavelengths from low energy radio to high energy γ -ray and on a broad range of timescales from hours to years (e.g., Wagner & Witzel 1995; Ulrich et al. 1997; Giveon et al. 1999; Kelly et al. 2009; MacLeod et al. 2010; Meusinger et al. 2011; Rakshit & Stalin 2017; Rumbaugh et al. 2018; Li et al. 2018), has been used to probe their central regions which are beyond the reach of any imaging techniques (Rakshit et al. 2015). Optical variability studies on large samples of AGN found interesting relations of the amplitude and timescale of variability with the physical parameters of AGN such as black hole mass, FeII strength, redshift etc. (e.g., di Clemente et al. 1996; Vanden Berk et al. 2004; Kelly et al. 2009; MacLeod et al. 2010; Meusinger et al. 2011; Rakshit & Stalin 2017; Li et al. 2018) providing new insights into the accretion process in AGN.

Various types of AGN are known and one among them are the narrow line Seyfert 1 (NLSy1) galaxies, which are classified based on the presence of narrow $H\beta$ emission line

* E-mail: suvenduat@gmail.com

† Project work carried out at IIA as part of the IASc-INSa-NASI Summer Research Fellowship -2017

with full width at half maximum (FWHM) $< 2000 \text{ km s}^{-1}$ and weak [O III] emission line, with $F([\text{O III}])/F(\text{H}\beta) < 3$ (Osterbrock & Pogge 1985; Goodrich 1989). They are believed to be powered by low mass black holes ($\sim 10^7 M_\odot$) having higher accretion rate and generally showing strong Fe II emission compared to their broad line counterparts namely the broad-line Seyfert 1 (BLSy1) galaxies (Xu et al. 2012; Rakshit et al. 2017a). However, from spectro-polarimetric observations of a γ -ray emitting NLSy1 galaxy, PKS 2004–447 (Baldi et al. 2016) and accretion disk modeling of a sample of 23 radio-detected NLSy1 galaxies (Calderone et al. 2013) indicate that they have masses similar to the blazar class of AGN. Other characteristics that make NLSy1 galaxies different from the BLSy1 galaxies are their rapid soft X-ray variability (Leighly 1999a; Pounds et al. 1995), steep soft X-ray spectra (Boller et al. 1996; Wang et al. 1996; Leighly 1999b) and low amplitude optical variability (Grupe 2004; Rakshit & Stalin 2017). Also, the fraction of NLSy1 galaxies detected in radio is much lower ($\sim 7\%$) compared to the fraction of radio detected BLSy1 galaxies (Komossa et al. 2006; Rakshit et al. 2017a). Among radio-loud NLSy1 galaxies, about a dozen ($\sim 2\%$) have been detected in γ -ray by the *Fermi*-Large Area Telescope (e.g., Abdo et al. 2009; D’Ammando et al. 2015; Paliya et al. 2018) suggesting the unambiguous presence of relativistic jets in them. Multi-band broad band SED modeling of these γ -ray detected NLSy1 galaxies indicate that these sources have many properties similar to the blazar class of AGN (Paliya et al. 2013b) and specifically resembling the flat spectrum radio quasar (FSRQ) category (Paliya et al. 2018). In the radio, these γ -ray emitting NLSy1 galaxies have a compact core jet morphology, high brightness temperature, show superluminal motion and significant radio variability (Komossa et al. 2006; Doi et al. 2006). Detailed investigations of the population of NLSy1 galaxies need to be undertaken to understand more about their peculiar characteristics.

The long-term (multi-year) optical variability nature of NLSy1 galaxies, compared to their broad line counterparts have been recently investigated by Rakshit & Stalin (2017), using a large number of sources from the catalog of Rakshit et al. (2017a) with the optical data taken from the Catalina Real Time Transient Survey (CRTS; Drake et al. 2009). In addition to the long-term optical variability, the intra-night optical variability characteristics of different categories of NLSy1 galaxies are also well studied (Liu et al. 2010; Paliya et al. 2013a; Kshama et al. 2017; Maune et al. 2013). However, studies on the IR variability characteristics of NLSy1 galaxies are very limited. Rapid variability in the IR bands has been seen in three radio-loud NLSy1 galaxies on intra-day timescales (Jiang et al. 2012). Studies of IR variability are important as IR echoes in response to the optical continuum variations, can provide very crucial information about the dust torus morphology and the accretion mechanism (Maune et al. 2013). Moreover, IR wavelengths have some unique advantages over optical wavelengths, for example (1) IR continuum is unaffected by the presence of strong emission lines in low redshift AGN and (2) less affected by dust extinction.

Given the limited studies on the IR variability characteristics of NLSy1 galaxies, a systematic study on an unbiased sample of sources is needed to give insight into their IR

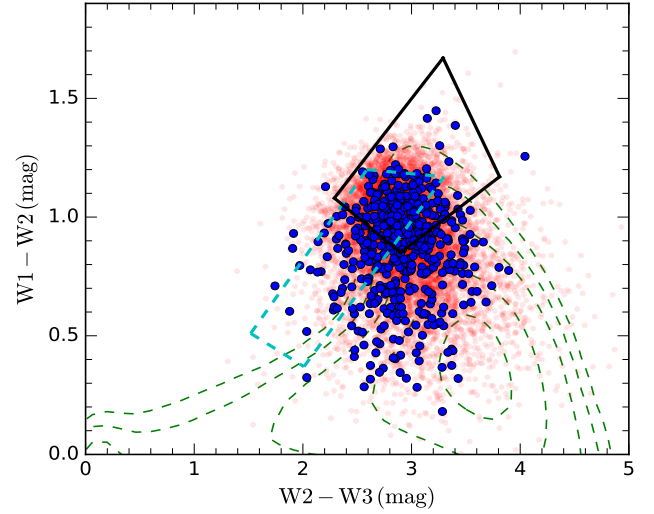


Figure 1. The *WISE* color-color diagram of the 520 variable candidates (blue circles) along with the parent NLSy1 galaxy sample (red dots). The *WISE* Gamma-ray strips for BL Lacs (dashed-cyan) and FSRQs (solid-black) is also shown. The green dashed contours represent *WISE* thermal sources (see text for explanation).

variability nature. We, therefore, have carried out a systematic investigation of the mid-IR flux variability characteristics of a sample of NLSy1 galaxies taken from the catalog of Rakshit et al. (2017a). This is the first large-scale statistical study of the IR variability of NLSy1 galaxies both in long-term as well as short-term (intra-day) containing few hundreds of sources. The sample and data used in this study are described in Section 2, our analysis is given in Section 3 and the summary of the results are presented in Section 4. A cosmology with $H_0 = 70 \text{ km s}^{-1} \text{ Mpc}^{-1}$, $\Omega_m = 0.3$, and $\Omega_\Lambda = 0.7$ is assumed throughout and all magnitudes from *WISE* used here are in the Vega System.

2 SAMPLE AND DATA

For this work, we have taken all NLSy1 galaxies from the catalog of Rakshit et al. (2017a), the selection of which was based on the spectroscopic database of the Sloan Digital Sky Survey Data Release 12 (SDSS DR12; Alam et al. 2015). The catalog consists of a total of 11,101 NLSy1 galaxies. Since the main motivation of this work is to characterize the IR variability properties of the population of NLSy1 galaxies, we looked for the IR counterparts to these sources in the *Wide-field Infrared Survey Explorer* (*WISE*; Wright et al. 2010) database. *WISE* has mapped the entire sky in four different IR bands centered at $3.4 \mu\text{m}$ (*W1* band), $4.6 \mu\text{m}$ (*W2* band), $12 \mu\text{m}$ (*W3* band) and $22 \mu\text{m}$ (*W4* band) with angular resolution of 6.1, 6.4, 6.5 and 12 arcsec, respectively. It has much higher sensitivity than any previous all sky surveys in IR. *WISE* has a field of view of $47 \text{ arcmin} \times 47 \text{ arcmin}$ and scans the entire sky once in every six months. The observations were performed (i) under *WISE* full cryogenic and NEOWISE Post-Cryo mission in three windows

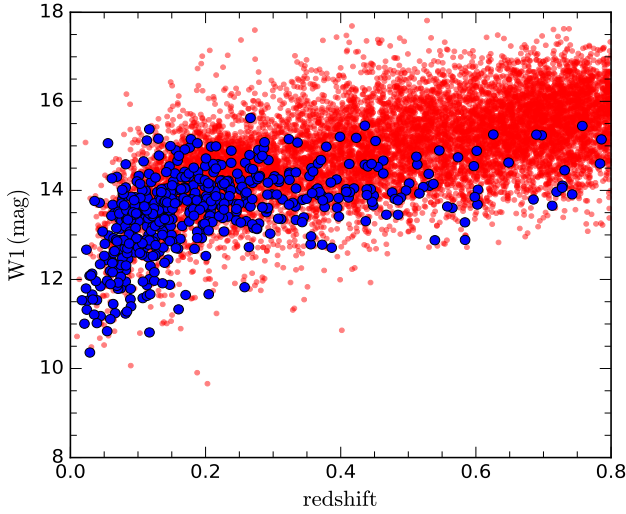


Figure 2. The $W1$ magnitude is plotted against the redshift of the 520 variable candidates (blue circles) along with the parent NLSy1 galaxy sample (red dots).

in 2010-2011 in $W1$, $W2$, $W3$ and $W4$ bands. All photometric magnitudes from this mission are included in the “AllWISE MultiEpoch Photometry (MEP) Database” and (ii) under the near-Earth objects *WISE* (NEOWISE) Reactivation mission (hereafter, NEOWISE-R; Mainzer et al. 2014) in 8 windows in 2014-2017 in $W1$ and $W2$ bands. All NEOWISE-R data are included in the “NEOWISE-R Single Exposure (L1b) Source Table”.

Within each visibility window, *WISE* observed sources continuously for a day, but sometimes more, with a cadence of 90 min, however, in some cases two exposures within 90 min were taken at 11s apart. The number of observations per window varied with ecliptic latitude. Thus, variability on short timescales of 90 minutes and long timescales of 6 months are most easily detected, but the observations are less sensitive to other timescales. Such a temporal sampling is suitable enough for short-term and long-term variability studies. The “AllWISE Source Catalog” contains data from the *WISE* cryogenic and NEOWISE post-cryogenic survey phases having about 747 million objects detected on the coadded atlas images. The catalog includes the variability flag, `var_flg`¹ from the observations done during 2010-2011. This flag, an integer value from 0 to 9, gives the probability of flux variation in each source. A value of 0 means no variability, while a value from 1 to 9 indicates increasing probability of variability (Hoffman et al. 2012).

We cross-correlated all the 11,101 NLSy1 galaxies from Rakshit et al. (2017a) with the “AllWISE Source Catalog” with a search radius of 2 arcsec centered at their optical position that resulted in 10,777 matches. From this list of 10,777 sources, we imposed the criteria of the `var_flg` equal to or greater than “3” since `var_flg` less than “3” can be considered as non-variable sources in the given band. The above

criteria led us to a sample of 520 objects. The position of these sources (blue circles) in the color-color ($W1$ - $W2$ - $W3$) diagram is shown in Figure 1. Also in the same figure, our initial sample of 10,777 NLSy1 galaxies (red dots) having IR detections in *WISE* is shown. The location of the *WISE* Gamma-ray strips (Massaro et al. 2012) for BL Lac and FSRQs are shown by the cyan dashed and black solid lines, respectively. The green dashed lines (see Cutri et al. 2011; Massaro et al. 2011) are the density contours of 364,994 *WISE* thermal sources in a region of 48 deg² area around high Galactic latitude ($l, b = 225^\circ, -55^\circ$) taken from the *WISE* Preliminary Release Source Catalog (WPSC). Interestingly, 57.6% of our sample of the 520 NLSy1 galaxies fall within the *WISE* Gamma-ray strips, of which 153 occupy the region populated both by BL Lacs and FSRQs. This similarity supports the detection of a handful of NLSy1 galaxies in γ -ray (Abdo et al. 2009; Paliya et al. 2018) but the detection might increase with the improvement in the sensitivity limit of future γ -ray instruments. Note that our sample of 520 sources has a mean $W1$ - $W2$ color of 0.99 ± 0.18 mag. In Figure 2, we show the distribution of $W1$ magnitude against SDSS spectroscopic redshift (see Rakshit et al. 2017a) for the parent NLSy1 galaxy sample (red) and 520 variable candidates (blue). About 87% of the variable candidates are located at $z < 0.4$ and all of them are brighter than 16 mag in $W1$ -band.

For quantitative variability analysis of our final sample of 520 NLSy1 galaxies, we combined data from “AllWISE MultiEpoch Photometry (MEP) Database” and NEOWISE-R allowing us to study about 7 years long light curves. Since $W3$ and $W4$ bands data are only available between 2010-2011 in one or two windows, and many photometric points are marked as “null”, which means no useful brightness estimate could be made, we, therefore, focus on data acquired only in $W1$ and $W2$ bands. To exclude bad photometric measurements available in the *WISE* database in $W1$ and $W2$ bands for these 520 objects we adopted the following criteria

- (i) The reduced χ^2 of single-exposure profile-fit is less than 5 in both $W1$ and $W2$ bands (i.e., `w1rchi2` < 5 and `w2rchi2` < 5),
- (ii) The number of point spread function (PSF) components used in profile fit for a source (`nb`) must be less than 3,
- (iii) The best quality single-exposure image (`qi_fact`=1), and frames are unaffected by known artifacts (`cc_flags`='0000') and are not actively deblended (`na`=0),
- (iv) The number of photometric measurements available in a day must be at least five. This condition was applied only for variability analysis within a day.

Using the above constraints, from our sample of 520 sources, we arrived at a final sample of 492 NLSy1 galaxies for further analysis. To study intra-day variability, we created the intra-day light curves by separating the photometric points into groups (hereafter “days”). One intra-day lightcurve includes all photometric data points having time gaps between two successive points lesser than 1.2 days. It is possible that the *WISE* images are affected by cosmic rays which are easily identifiable as outliers in the photometric light curves of an object. Therefore, we applied a 3σ (where σ is the standard deviation of the light curve) clipping to each

¹ For more information about `var_flg` see http://wise2.ipac.caltech.edu/docs/release/allwise/expsup/sec5_3bvi.html

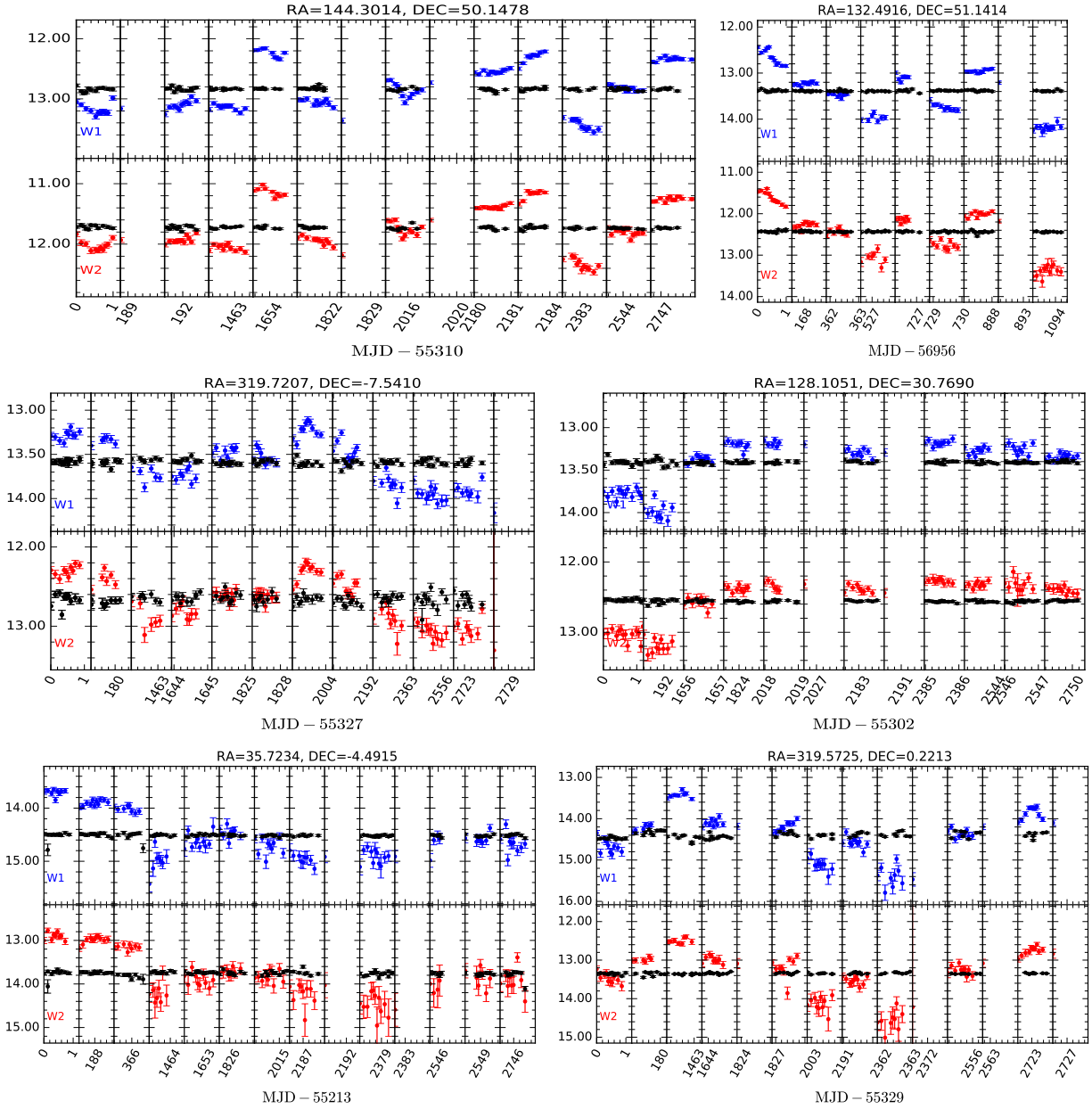


Figure 3. Examples of *WISE* multi-epoch light curves in W1 (upper-panel) and W2 bands (lower-panel) for six NLSy1 galaxies (from top to bottom: 3FGL J0937.7+5008, 3FGL J0849.9+5108, SDSS J211852.96-073227.5, 2MASX J08322525+3046090, SDSS J022253.61-042929.2, 3FGL J2118.4+0013). The magnitudes of the objects in the Vega system are plotted along Y-axis. The light curve of a nearby star (magnitudes 8.4, 9.5, 12.2, 9.3, 11.6, 7.2 respectively from top to bottom in W1 band) present in the same field is also shown (black) after shifting by a constant value for comparison. The NLSy1 galaxies show large long-term variation compared to the stars. Each subplot has a size of 1.2 days.

intra-day light curve to remove photometric outliers usually present in the survey data. We found that majority of the light curves do not have any outliers while in some cases they are present but such number of outliers are usually one in a light curve which were removed by our 3σ clipping. Thus, the light curves used in the analysis were devoid of the effects of cosmic ray hits. We visually inspected those light curves before removing the outliers. We also noticed that in many light curves photometric points were present with a separation of only about 11s in successive WISE epochs.

Since the duration of the *WISE* orbit is about 1.5 hours, we took the mean of the photometric points available within 1.5 hours and constructed the light curve. Sample light curves for six sources in W1 and W2 bands are shown in Figure 3 with each box representing a duration of 1.2 days. The light curve of a nearby star present in the same field is over plotted (after shifting by a constant value for the purpose of comparison) along with the light curve of NLSy1 galaxies. The variation of stars are constant over short and long-term while NLSy1 galaxies show large amplitude of variability.

The number of windows in a light curve varies from 2 to 14 with a median of 10, while the total number of points range from 9 to 471 with a median of 108.

For all objects, if intra-day light curves have more than five photometric data points, we considered them for short-term variability analysis. The intra-day light curves used in this analysis thus consisted of a minimum of 5 and maximum of about 86 photometric points while long-term light curves are very sparsely sampled. In some of the windows, the number of photometric points can be as low as one because of the other photometric points if any not satisfying the criteria mentioned above. Though such windows were not considered for intra-day variability analysis, they were considered for long-term variability analysis. Such sparsely sampled light curves prevented us to perform any time series analysis, such as auto-correlation analysis to estimate the correlation timescale or cross-correlation analysis between *W1* and *W2* bands to estimate the relative size of emitting regions. Thus, in this work, we focused only on the amplitude of variability in *W1* and *W2* bands.

3 ANALYSIS

3.1 Flux variability

To quantitatively study variability, we calculated the intrinsic amplitude of variability (σ_m), which is the variance of the observed light curve after removing the measurement uncertainty (see also Rakshit & Stalin 2017). The σ_m is calculated using the following formalism described in Sesar et al. (2007).

$$\Sigma = \sqrt{\frac{1}{n-1} \sum_{i=1}^N (m_i - \langle m \rangle)^2}, \quad (1)$$

where m_i is the magnitude at i -th point and $\langle m \rangle$ is the weighted average. The amplitude of variability can be written as σ_m is

$$\sigma_m = \begin{cases} \sqrt{\Sigma^2 - \epsilon^2}, & \text{if } \Sigma > \epsilon, \\ 0, & \text{otherwise.} \end{cases}$$

where the error ϵ is calculated from the individual errors as follows

$$\epsilon^2 = \frac{1}{N} \sum_{i=1}^N \epsilon_i^2 + \epsilon_s^2. \quad (2)$$

Here ϵ_i is the measurement uncertainty of i -th point and ϵ_s is the systematic uncertainty. Jarrett et al. (2011) reported systematic uncertainties of 0.024 mag and 0.028 mag in *W1* and *W2* respectively. Therefore, this error has been added in quadrature to the measurement uncertainty and thus taking care of systematic as well as random errors. Spurious correlation may occur if σ_m is not corrected for the redshift of the object, especially important for a flux-limited sample, we, therefore, calculated rest frame σ_m by multiplying σ_m with $\sqrt{(1+z)}$, which is based on the power spectral density of variability having slope 2 (see Kelly et al. 2009). However, the majority ($\sim 87\%$) of the variable candidates in our sample is below $z = 0.4$, thus, redshift correction is insignificant.

3.1.1 Long-term variability amplitude

Variability information of all the 492 candidate variables are provided in Table 1. We found that in the long-term 483 and 473 NLSy1 galaxies have $\sigma_m > 0$ in the *W1* and *W2* bands respectively. Among these, 473 NLSy1 galaxies² have $\sigma_m > 0$ both in *W1* and *W2* bands. The σ_m in *W1* band is plotted against *W1* magnitude in Figure 4 on the left panel whereas the distributions of σ_m in *W1* and *W2* bands are shown in the right panel. The average σ_m is 0.11 ± 0.07 mag (0.11 ± 0.08 mag) in *W1* (*W2*) band. Thus, there seems to be no difference in the amplitude of flux variations in *W1* and *W2*. This has also been confirmed by a two-sample KS test. Rakshit & Stalin (2017) estimated long-term variability in *V*-band for a large sample of NLSy1 and BLSy1 galaxies. Cross-matching our sample with them, we found that 142 NLSy1 galaxies are common to this work and Rakshit & Stalin (2017). The average long-term optical variability of these 142 NLSy1 galaxies is 0.11 mag similar to that of their average long-term *W1* band variability, which is 0.11 mag.

3.1.2 Short-term variability amplitude

Figure 3 shows examples of light curves in which the short-term flux variations in some objects at some windows are visible. Firstly, the amplitude of short-term variations are quite low compared to the long-term variations and secondly, in many cases, there is no one to one correspondence (both in the pattern and amplitude) between the short-term variations in *W1* and *W2* bands. Such lack of one to one correspondence precludes us to use all the intra-day light curves for short-term variability analysis. Therefore, to quantify short-term variability we calculated the variability covariance (see Kozłowski et al. 2016; Polimera et al. 2018) as

$$C_{12} = \frac{1}{N-1} \sum_{i=1}^N (m[W1]_i - \langle m[W1] \rangle)(m[W2]_i - \langle m[W2] \rangle) \quad (3)$$

and Pearson's correlation coefficient of variability between *W1* and *W2* bands as

$$r_{12} = \frac{C_{12}}{\Sigma_{W1} \Sigma_{W2}} \quad (4)$$

The value of r_{12} ranges from -1 (perfect anti-correlation) to 1 (perfect correlation). A truly variable light curve should have high correlation. Thus, we considered a short-term light curve is variable if $\sigma_m > 0$ and $r_{12} > 0.8$ (Kozłowski et al. 2016; Polimera et al. 2018). For a given object, we then calculated average variability from the light curves having $\sigma_m > 0$ and $r_{12} > 0.8$ as a representation of the intra-day variability for that object. Only 31 and 24 objects showed short-term variability in at least one window in *W1* and *W2* bands respectively while only 17 objects showed short-term variability in both *W1* and *W2* bands.

We also estimated the duty cycle (DC; see Rakshit et al. 2017b) i.e. the fraction of time when an object is variable in

² Light curves of all the 473 NLSy1 galaxies along with the values of their long-term variability amplitude in *W1* and *W2* bands can be obtained in the electronic version of the paper.

Table 1. Variability information. The columns are as follows: (1) SDSS ID (plate-mjd-fiber), (2) RA (degree), (3) DEC (degree), (4) redshift, (5) $\log \lambda L_{5100}$ (erg s^{-1}), (6) number of points in $W1$ band light curve, (7) number of points in $W2$ band light curve, (8) number of short-term light curves with minimum 5 points in both $W1$ and $W2$ bands, (9) average $W1$ -band magnitude, (10) average $W2$ -band magnitude, (11) variability amplitude in $W1$ -band (mag), (12) variability amplitude in $W2$ -band (mag), and (13) radio power (erg s^{-1}). This table is available in its entirety in machine-readable form. A portion is shown here for guidance.

SDSS ID	RA	DEC	z	$\log \lambda L_{5100}$	N_p ($W1$)	N_p ($W2$)	N_{lc}	$\langle W1 \rangle$	$\langle W2 \rangle$	$\sigma_m(W1)$	$\sigma_m(W2)$	$\log P_{1.4GHz}$
(1)	(2)	(3)	(4)	(5)	(6)	(7)	(8)	(9)	(10)	(11)	(12)	(13)
2004-53737-0466	182.4384	32.2836	0.1447	44.04	96	97	9	12.64	11.63	0.16	0.13	39.18
0873-52674-0158	155.5400	48.3538	0.0626	42.85	54	54	3	13.70	13.29	0.09	0.13	...
0443-51873-0092	127.7197	48.3332	0.2233	43.19	107	107	9	14.14	13.18	0.26	0.22	...

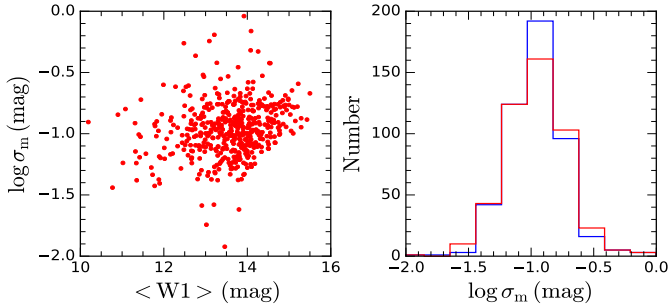


Figure 4. Left: Variability amplitude in $W1$ band in the long-term against mean $W1$ magnitude. Right: The distributions of variability amplitude in $W1$ (blue) and $W2$ (red) bands.

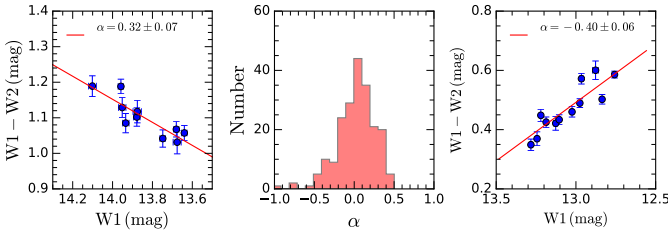


Figure 5. Long-term color variation: an example of bluer when brighter trend (left), the distribution of slope of the objects in our sample (middle) and an example of redder when brighter trend (right).

intra-day timescale following [Romero et al. \(1999\)](#),

$$DC = 100 \frac{\sum_{i=1}^n N_i (1/\Delta t_i)}{\sum_{i=1}^n (1/\Delta t_i)} \%, \quad (5)$$

where $\Delta t_i = \Delta t_{i,obs}(1+z)^{-1}$ is the rest frame duration of the monitoring session of the source on the i -th light curve and n is the maximum number of short-term light curves in a given object. If $\sigma_m > 0$ and $r_{12} > 0.8$ in a short-term light curve then $N_i = 1$ else $N_i = 0$. The DC for those 17 objects having short-term variation in both the $W1$ and $W2$ bands ranges from 6% to 67% with a median of 11%. The highest DC of 67% is observed in 3FGL J0948.8+0021, which is a γ -ray emitting NLSy1 galaxy.

3.2 Color variation in long-term

To investigate color variation in long-term, we calculated the mean color ($\langle W1 - W2 \rangle$) and the mean $W1$ magnitude ($\langle W1 \rangle$) by taking the mean of all the data points in each short-term light curves. An example of the fitting to the long-term color-magnitude relation for a NLSy1 galaxy is shown in Figure 5 (left panel), which shows bluer when brighter (BWB) trend. We performed linear fits to the color-magnitude relation taking into account the errors on both axes and calculated the Pearson rank correlation coefficient (r_p) between color-magnitude relation of the 232 sources having $\sigma_m > 0.1$ mag in the long-term. We plot the distribution of the slope (α) of 206 sources, which has $|r_p| > 0.8$, in the middle panel. The distribution of α has a mean of 0.05 with a dispersion of 0.24. We note a mean uncertainty of 0.1 in the measurement of α . Thus, the dispersion among true source α values is ~ 0.22 .

About 31% sources show no color variation within the 1σ measurement uncertainty. Among the rest of the 69% sources, 42% show BWB trend while 27% exhibit redder when brighter (RWB) trend. One example of RWB trend seen in a NLSy1 galaxy is shown in the right panel of Figure 5. The observed IR emission is predominantly due to reprocessed UV/optical emission by the torus. The total observed UV/optical flux is a sum of a constant component that comes from stars in the host galaxy and a variable component from the central nuclear region of AGN. For AGN, with no dilution due to star light from host galaxies, $W1 - W2$ colors are redder upto $z \sim 3.5$, however, an increased contribution of star light will lead to bluer $W1 - W2$ colors ([Stern et al. 2012](#)). When the variable nuclear component is dominant, the constant host galaxy component will have little effect on the total observed flux. The increased brightness of the AGN can thus lead to a strong contribution by the AGN dust torus to the observed IR emission leading to a redder $W1 - W2$ color when the AGN is brighter. Alternatively, the host galaxy light can play a role to the observed flux only when the AGN fades and the AGN central nuclear luminosity becomes comparable to the host galaxy stellar brightness, which could lead to a BWB trend ([Yang et al. 2018](#)).

3.3 Dependence of color and long-term variability on AGN parameters

To study the correlation of long-term variability amplitude with AGN parameters, we calculated the black hole mass (M_{BH}), bolometric luminosity (L_{BOL}) and Eddington luminosity (L_{Edd}) based on the spectral fitting results of [Rakshit et al. \(2017a\)](#) following [Rakshit & Stalin \(2017\)](#). First, the

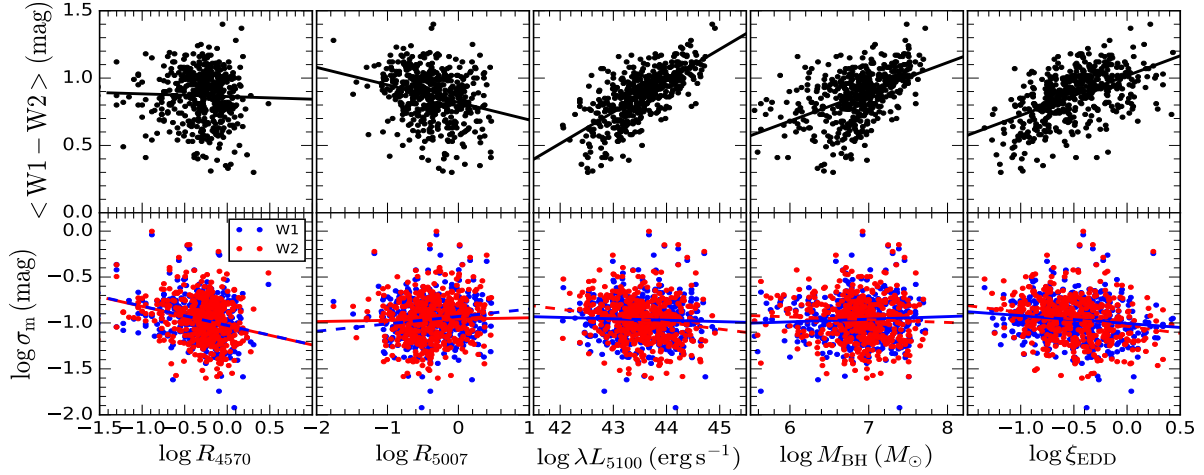


Figure 6. Correlation of average long-term color $\langle W1 - W2 \rangle$ (upper panels) and long-term σ_m (lower panels) with R_{4570} , R_{5007} , λL_{5100} , M_{BH} , ξ_{Edd} are plotted from left to right columns respectively. The straight lines represent linear fits to the relations. In the lower panel, σ_m for W1 (blue) and W2 bands (red) are plotted.

Table 2. Correlation of average color and long-term σ_m with different AGN parameters. The columns are as follows: (1) test parameter. Columns (2)–(6) note the Spearman correlation coefficient r_s (the p -value of no correlation) for $\log R_{4570}$, $\log R_{5007}$, $\log \lambda L_{5100}$, $\log M_{BH}/M_{\odot}$ and $\log \xi_{Edd}$.

Test parameter (1)	$\log R_{4570}$ (2)	$\log R_{5007}$ (3)	$\log \lambda L_{5100}$ (4)	$\log M_{BH}/M_{\odot}$ (5)	$\log \xi_{Edd}$ (6)
$\langle W1 - W2 \rangle$	-0.05 (2e-01)	-0.28 (3e-10)	+0.69 (2e-72)	+0.51 (6e-35)	+0.54 (3e-38)
$\log \sigma_m$ (W1)	-0.28 (7e-10)	+0.03 (5e-01)	-0.06 (1e-01)	+0.00 (5e-01)	-0.14 (1e-03)
$\log \sigma_m$ (W2)	-0.24 (1e-07)	+0.13 (4e-03)	-0.18 (3e-05)	-0.08 (7e-02)	-0.21 (2e-06)

size of the broad line region (R_{BLR}) was calculated based on the size-luminosity scaling relation obtained by Bentz et al. (2013). Then assuming virial relationship and spherical distribution of clouds (virial scale factor, $f = 3/4$), the black hole mass of each source was calculated using the full width at half maximum of the broad component of $H\beta$ emission line (Δv), $M_{BH} = f R_{BLR} \Delta v^2 / G$. The L_{BOL} was approximated as $L_{BOL} = 9 \times \lambda L_{\lambda}(5100) \text{ erg s}^{-1}$ and L_{Edd} was calculated as $L_{Edd} = 1.3 \times 10^{38} M_{BH}/M_{\odot} \text{ erg s}^{-1}$ (Kaspi et al. 2000). The Eddington ratio is given by $\xi_{Edd} = L_{BOL}/L_{Edd}$. The values of Fe II strength (R_{4570}) i.e., the flux ratio of Fe II to $H\beta$ and R_{5007} (defined by the flux ratio of [O III] to total $H\beta$) were taken from Rakshit et al. (2017a).

In Figure 6, we performed several correlations to understand the dependency of mean long-term $W1 - W2$ color (upper panels) and long-term variability amplitude σ_m (lower panels) with various physical parameters of the NLSy1 galaxies in our sample such as R_{4570} , R_{5007} , λL_{5100} , M_{BH} and ξ_{Edd} . Linear least square fits (indicated by straight lines) carried out on the data are shown in Figure 6 and the results of the Spearman rank correlation analysis are summarized in Table 2 where correlation coefficient (r_s) and the p -value of no correlation is given. We found no correlation between $W1 - W2$ and R_{4570} , however, $W1 - W2$ color is inversely correlated with R_{5007} having $r_s = -0.28$. The λL_{5100} , M_{BH} and ξ_{Edd} are strongly correlated with $W1 - W2$ color having $r_s = +0.69$, $+0.51$ and $+0.54$ respectively.

Figure 6 (top panel) shows a strong trend for more lumi-

nous objects to be redder. Firstly, the continuum luminosity at 5100\AA was from the optical spectra (stellar contribution subtracted) of the sources and in that epoch, the object can be of any brightness level (faint, moderate or bright). Secondly, the $\langle W1 - W2 \rangle$ color is the average $W1 - W2$ of all the points in a particular object. Thus the middle panels of Figure 6 depict the average behavior of the NLSy1 galaxy population in $W1 - W2$ versus 5100\AA luminosity. Thus on average brighter NLSy1 galaxies have redder $W1 - W2$ color. Such a behavior is caused by a larger contribution of the dust torus to the observed IR emission at bright flux levels of NLSy1 galaxies (Yang et al. 2018).

We also investigated the correlation between the $W1 - W2$ color against various emission line parameters of the sources. We found an inverse correlation between $W1 - W2$ versus R_{5007} , which agrees with the findings of Chen et al. (2017). Between $W1 - W2$ and R_{4570} we found no correlation, however, Chen et al. (2017) noticed a weak positive correlation between $W1 - W2$ and R_{4570} . From Rakshit et al. (2017a) using their complete sample of NLSy1 galaxies it is known that both the luminosity of $H\beta$ and [O III] lines correlate positively with the continuum luminosity at 5100\AA as

$$\log L(H\beta_{tot}) = -(4.30 \pm 0.21) + (1.056 \pm 0.004) \log \lambda L_{5100} \quad (6)$$

where $L(H\beta_{tot})$ is the total $H\beta$ luminosity, and

$$\log L[\text{OIII}] = (9.87 \pm 0.29) + (0.721 \pm 0.006) \log \lambda L_{5100}. \quad (7)$$

Rearranging equations 6 and 7 we found

$$\log R_{5007} = (14.17 \pm 0.35) - (0.335 \pm 0.007) \log \lambda L_{5100} \quad (8)$$

Thus, on average NLSy1 galaxies at higher optical luminosities have lower R_{5007} and redder $W1 - W2$. The different relation of $W1 - W2$ color versus R_{4570} and $W1 - W2$ color versus R_{5007} is not surprising considering their origin. The [O III] emission comes from the narrow line region, while Fe II and H β originate in the BLR.

The correlation of σ_m in the long-term light curve of $W1$ (blue) and $W2$ (red) bands is plotted with R_{4570} , R_{5007} , λL_{5100} , M_{BH} and ξ_{Edd} in the lower panel of Figure 6. There is a weak negative correlation between σ_m in long-term $W1$ and $W2$ light curves with R_{4570} , λL_{5100} and ξ_{Edd} . The results of the Spearman rank correlation analysis are given in Table 2. This plot can be compared with the Figure 8 of Rakshit & Stalin (2017), where the correlation of σ_m in optical has been plotted with the same parameters. Interestingly, the correlations which are present in the optical are also present here though weaker. This could be simply due to the different origin of near-IR variability than optical. However, note that *WISE* light curves are very sparsely sampled thus local monthly variation cannot be probed.

The optical continuum originates from the accretion disk while near-IR continuum is mainly due to the radiation from a dusty torus beyond the dust sublimation radius (Laor & Draine 1993). The optical and IR emissions are causally connected and it is not surprising that the correlations between variability and various physical characteristics of the sources seen in the optical bands are also seen in the IR bands. The ξ_{Edd} , which is considered to be the main driver of optical variability inversely correlates with the σ_m in optical (see Kelly et al. 2009; MacLeod et al. 2010; Meusinger et al. 2011; Rakshit & Stalin 2017). Such an inverse correlation could be explained using simple standard accretion disk model (Shakura & Sunyaev 1973). The radius (R in the unit of the Schwarzschild radius) of the emission region increases with Eddington ratio for a given wavelength, $R \sim T^{-4/3} \sim (\dot{m}/M_{BH})^{1/3} \lambda^{4/3}$, λ is the wavelength of observation and \dot{m} is the mass accretion rate in the unit of Eddington rate. At any given wavelength, for a high Eddington ratio object, the primary emission comes from the outer region of the accretion disk, compared to a low Eddington ratio object, where the primary emission comes from the inner region of the accretion disk. Thus it is natural to expect an anti-correlation between variability amplitude and Eddington ratio. However, as the observed IR emission is the reprocessed primary emission from the accretion disk, the observed variability is diluted and therefore the anticorrelation between σ_m and λ_{Edd} is much weaker in the IR than optical.

3.4 Variability of radio subsample

In the population of NLSy1 galaxies, a minority of about 7% are radio-loud (Komossa et al. 2006; Rakshit et al. 2017a). To understand the influence of radio emission on the observed color and IR flux variations, we performed a comparative analysis of the color and flux variability characteristics of radio-quiet and radio-loud NLSy1 galaxies. Towards this, we cross-correlated our sample of NLSy1 galaxies with the

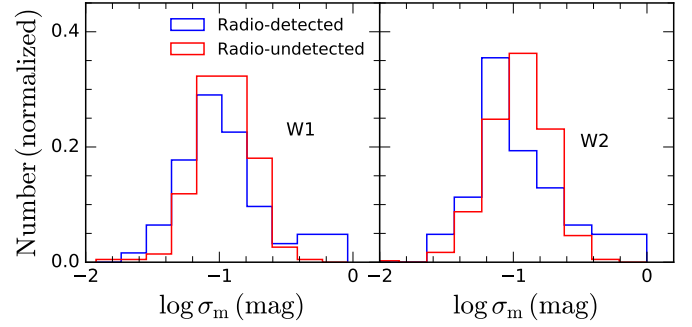


Figure 7. Distribution of long-term variability amplitude of radio-detected (blue) and radio-undetected (red) NLSy1 galaxies.

FIRST (Faint Images of the Radio Sky at Twenty cm) catalog (Becker et al. 1995). This leads us to 63 radio-detected NLSy1 galaxies.

The distribution of σ_m for radio-detected and radio-undetected NLSy1 galaxies are plotted in Figure 7. Considering long-term variability, the mean σ_m is 0.16 ± 0.16 mag and 0.12 ± 0.06 mag for the radio-detected and undetected sample respectively both in $W1$ and $W2$ bands. A two-sample KS test also confirms a marginal difference in the IR variability between radio-detected and radio-undetected NLSy1 galaxies having a D -statistics value 0.15 (p -value=0.17) and 0.18 (p -value=0.06) in the long-term in $W1$ and $W2$ bands. We plot in Figure 8 (left panel) the mean $W1 - W2$ color of radio detected NLSy1 galaxies against their radio power at 1.4 GHz ($P_{1.4\text{GHz}}$). A positive correlation is found with a Spearman correlation coefficient $r_s = 0.5$ and p -value= $3e - 5$ respectively. A positive correlation (right panel) is also found between the long-term variability amplitude and radio power at 1.4 GHz with $r_s = 0.33$ ($r_s = 0.40$) and p -value= $7e - 03$ ($1e - 03$) for $W1$ ($W2$) bands respectively. Note that a similar correlation between long-term variability amplitude and radio power has also been observed in the optical band (Rakshit & Stalin 2017). Interestingly, 9 objects with radio power $P_{1.4\text{GHz}} > 10^{41} \text{ergs}^{-1}$ exhibit stronger variability with $\sigma_m > 0.2$ mag (also see Figure 7). This includes 8 γ -ray emitting NLSy1 galaxies detected by *Fermi*-Large Area Telescope. Thus, though the major component of the IR variation in NLSy1 galaxies is the dusty torus, in the case of radio-detected NLSy1 galaxies, non-thermal jet emission too contributes to the observed IR emission as found from the strong trend of increasing variability amplitude with radio power.

4 SUMMARY

We have carried out a systematic analysis of the IR color and flux variability of a large sample of NLSy1 galaxies in two IR bands, namely $W1$ and $W2$. We find only $\sim 5\%$ of the initial WISE detected sample of 10,777 NLSy1 galaxies show detectable variability. The main findings of the color and variability analysis of the variable NLSy1 galaxies are summarized below

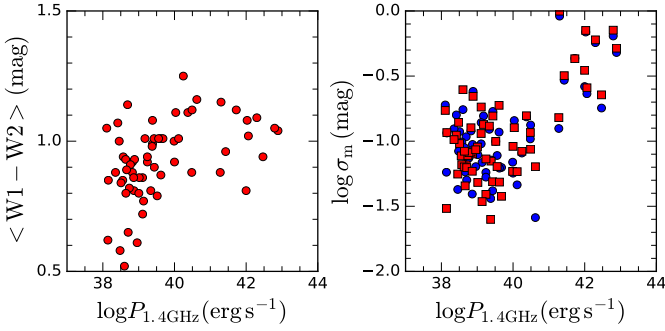


Figure 8. Correlation between mean $W1 - W2$ color versus $P_{1.4\text{GHz}}$ (left) and σ_m versus $P_{1.4\text{GHz}}$ in long-term (right). The circles and squares in the right panel represent $W1$ and $W2$ bands respectively.

- In the *WISE* color-color diagram, 57.6% objects of the 520 candidate variable NLSy1 galaxies fall within the WISE Gamma-ray strips having a mean $W1 - W2$ color of 0.99 ± 0.18 mag.

- In long-term, the mean amplitude of variability in $W1$ and $W2$ bands is 0.11 ± 0.07 mag and 0.11 ± 0.08 mag respectively. The amplitude of variability on long (year like) timescales is larger than that obtained on short timescales. The long-term IR variability characteristics of NLSy1 galaxies is similar to their long-term optical variability characteristics (Rakshit & Stalin 2017). This is expected as the observed IR emission is the re-processed optical/UV emission from the central engine of NLSy1 galaxies.

- The average $W1 - W2$ color is anti-correlated with R_{5007} but strongly correlated with λL_{5100} , M_{BH} and ξ_{Edd} . However, no correlation was found between $W1 - W2$ color and R_{4570} .

- Weak negative correlation was observed between σ_m with R_{4570} , λL_{5100} , and ξ_{Edd} in long-term. This is similar to what has been noticed in the optical band though here the correlations are much weaker compared to the optical. Densely sampled long-term light curves could provide more insights into the underlying physics of IR flux variation.

- The radio-detected NLSy1 galaxies on average showed similar variability compared to the radio-undetected sample. Considering only the radio-detected NLSy1 galaxies, a positive correlation is found between the mean $W1 - W2$ color and the radio power at 1.4 GHz. A total of 9 objects with radio power $P_{1.4\text{GHz}} > 10^{41}$ erg s $^{-1}$, which includes 8 γ -ray emitting NLSy1 galaxies exhibit stronger variability ($\sigma_m > 0.2$ mag). Also, for the same sample, a positive correlation is noticed between the amplitude of variability and the 1.4 GHz radio power. This points to the possible contribution of jet emission to the observed IR emission in the radio-detected NLSy1 galaxies.

5 ACKNOWLEDGMENTS

We thank the referee for his valuable comments and suggestions which helped to improve the manuscript. S.R. acknowledges the support by the Basic Science Research Program through the National Research Foundation of Korea

government (2016R1A2B3011457). A.J. thanks the Science Academies, for the fellowship provided to her to carry out a summer project at IIA from the IASc-INSa-NASI Summer Research Fellowship – 2017. S.R. thanks Neha Sharma (KHU, South Korea) for carefully reading the manuscript. This publication makes use of data products from the Wide-field Infrared Survey Explorer, which is a joint project of the University of California, Los Angeles, and the Jet Propulsion Laboratory/California Institute of Technology, funded by the National Aeronautics and Space Administration.

REFERENCES

- Abdo A. A., et al., 2009, *ApJ*, **699**, 976
 Alam S., et al., 2015, *ApJS*, **219**, 12
 Antonucci R., 1993, *ARA&A*, **31**, 473
 Baldi R. D., Capetti A., Robinson A., Laor A., Behar E., 2016, *MNRAS*, **458**, L69
 Becker R. H., White R. L., Helfand D. J., 1995, *ApJ*, **450**, 559
 Bentz M. C., et al., 2013, *ApJ*, **767**, 149
 Boller T., Brandt W. N., Fink H., 1996, *A&A*, **305**, 53
 Calderone G., Ghisellini G., Colpi M., Dotti M., 2013, *MNRAS*, **431**, 210
 Chen P. S., Liu J. Y., Shan H. G., 2017, *New Astron.*, **54**, 30
 Cutri R. M., et al., 2011, Technical report, Explanatory Supplement to the WISE Preliminary Data Release Products
 D’Ammando F., Orienti M., Larsson J., Giroletti M., 2015, *MNRAS*, **452**, 520
 Doi A., Nagai H., Asada K., Kamenos S., Wajima K., Inoue M., 2006, *PASJ*, **58**, 829
 Drake A. J., et al., 2009, *ApJ*, **696**, 870
 Givon U., Maoz D., Kaspi S., Netzer H., Smith P. S., 1999, *MNRAS*, **306**, 637
 Goodrich R. W., 1989, *ApJ*, **342**, 224
 Grupe D., 2004, *AJ*, **127**, 1799
 Hoffman D. I., Cutri R. M., Masci F. J., Fowler J. W., Marsh K. A., Jarrett T. H., 2012, *AJ*, **143**, 118
 Jarrett T. H., et al., 2011, *ApJ*, **735**, 112
 Jiang N., et al., 2012, *ApJ*, **759**, L31
 Kaspi S., Smith P. S., Netzer H., Maoz D., Jannuzi B. T., Givon U., 2000, *ApJ*, **533**, 631
 Kelly B. C., Bechtold J., Siemiginowska A., 2009, *ApJ*, **698**, 895
 Komossa S., Voges W., Xu D., Mathur S., Adorf H.-M., Lemson G., Duschl W. J., Grupe D., 2006, *AJ*, **132**, 531
 Koshida S., et al., 2014, *ApJ*, **788**, 159
 Kozłowski S., Kochanek C. S., Ashby M. L. N., Assef R. J., Brodwin M., Eisenhardt P. R., Jannuzi B. T., Stern D., 2016, *ApJ*, **817**, 119
 Kshama S. K., Paliya V. S., Stalin C. S., 2017, *MNRAS*, **466**, 2679
 Laor A., Draine B. T., 1993, *ApJ*, **402**, 441
 Leighly K. M., 1999a, *ApJS*, **125**, 297
 Leighly K. M., 1999b, *ApJS*, **125**, 317
 Li Z., McGreer I. D., Wu X.-B., Fan X., Yang Q., 2018, preprint, ([arXiv:1805.07747](https://arxiv.org/abs/1805.07747))
 Liu H., Wang J., Mao Y., Wei J., 2010, *ApJ*, **715**, L113
 Lynden-Bell D., 1969, *Nature*, **223**, 690
 MacLeod C. L., et al., 2010, *ApJ*, **721**, 1014
 Mainzer A., et al., 2014, *ApJ*, **792**, 30
 Mandal A. K., et al., 2018, *MNRAS*, **475**, 5330
 Massaro F., D’Abrusco R., Ajello M., Grindlay J. E., Smith H. A., 2011, *ApJ*, **740**, L48
 Massaro F., D’Abrusco R., Tosti G., Ajello M., Gasparrini D., Grindlay J. E., Smith H. A., 2012, *ApJ*, **750**, 138
 Maune J. D., Miller H. R., Eggen J. R., 2013, *ApJ*, **762**, 124
 Meusinger H., Hinze A., de Hoon A., 2011, *A&A*, **525**, A37

- Osterbrock D. E., Pogge R. W., 1985, [ApJ](#), **297**, 166
- Paliya V. S., Stalin C. S., Kumar B., Kumar B., Bhatt V. K., Pandey S. B., Yadav R. K. S., 2013a, [MNRAS](#), **428**, 2450
- Paliya V. S., Stalin C. S., Shukla A., Sahayanathan S., 2013b, [ApJ](#), **768**, 52
- Paliya V. S., Ajello M., Rakshit S., Mandal A. K., Stalin C. S., Kaur A., Hartmann D., 2018, [ApJ](#), **853**, L2
- Polimera M., Sarajedini V., Ashby M. L. N., Willner S. P., Fazio G. G., 2018, [MNRAS](#), **476**, 1111
- Pounds K. A., Done C., Osborne J. P., 1995, [MNRAS](#), **277**, L5
- Rakshit S., Stalin C. S., 2017, [ApJ](#), **842**, 96
- Rakshit S., Petrov R. G., Meilland A., Hönig S. F., 2015, [MNRAS](#), **447**, 2420
- Rakshit S., Stalin C. S., Chand H., Zhang X.-G., 2017a, [ApJS](#), **229**, 39
- Rakshit S., Stalin C. S., Muneer S., Neha S., Paliya V. S., 2017b, [ApJ](#), **835**, 275
- Rees M. J., 1984, [ARA&A](#), **22**, 471
- Romero G. E., Cellone S. A., Combi J. A., 1999, [A&AS](#), **135**, 477
- Rumbaugh N., et al., 2018, [ApJ](#), **854**, 160
- Sesar B., et al., 2007, [AJ](#), **134**, 2236
- Shakura N. I., Sunyaev R. A., 1973, [A&A](#), **24**, 337
- Stern D., et al., 2012, [ApJ](#), **753**, 30
- Suganuma M., et al., 2006, [ApJ](#), **639**, 46
- Ulrich M.-H., Maraschi L., Urry C. M., 1997, [ARA&A](#), **35**, 445
- Urry C. M., Padovani P., 1995, [PASP](#), **107**, 803
- Vanden Berk D. E., et al., 2004, [ApJ](#), **601**, 692
- Wagner S. J., Witzel A., 1995, [ARA&A](#), **33**, 163
- Wang T., Brinkmann W., Bergeron J., 1996, [A&A](#), **309**, 81
- Wright E. L., et al., 2010, [AJ](#), **140**, 1868
- Xu D., Komossa S., Zhou H., Lu H., Li C., Grupe D., Wang J., Yuan W., 2012, [AJ](#), **143**, 83
- Yang Q., et al., 2018, [ApJ](#), **862**, 109
- di Clemente A., Giallongo E., Natali G., Trevese D., Vagnetti F., 1996, [ApJ](#), **463**, 466